*Oil & Gas Science and Technology – Rev. IFP*, Vol. 56 (2001), No. 1, pp. 23-31


# Spreading of Large Drops on Patterned Surfaces

T. Cubaud[1], M. Fermigier[1] and P. Jenffer[1]

1 CNRS, UMR 7636, Laboratoire PMMH, ESPCI, 10, rue Vauquelin, 75231 Paris Cedex 05 - France
e-mail: fermi@pmmh.espci.fr

**Résumé — Étalement de grosses gouttes sur surfaces modèles** — Nous présentons une étude expérimentale de la forme de grosses gouttes posées sur des surfaces planes de mouillabilité contrôlée. Les substrats sont en partie recouverts de disques de matériaux moins mouillants que le reste de la surface : les défauts. Lorsque peu de défauts sont présents, ou que la distance moyenne entre deux défauts est supérieure à la longueur capillaire, la ligne de contact est une succession d'arcs de cercle connectés aux points d'accrochage formés par les défauts. Lorsque la distance moyenne entre défauts est inférieure à la longueur capillaire, la forme de la ligne de contact est plus complexe et nous analysons sa morphologie en calculant le périmètre des gouttes avec des règles de longueurs variables. La rugosité de la ligne de contact est maximale pour une distance moyenne entre défauts de l'ordre de deux fois la taille des défauts. L'étalement d'un liquide sur un substrat dont les défauts sont distribués en réseau périodique, ou presque, produit une goutte à bords facettés. La transition entre gouttes facettées et gouttes circulaires peut être comprise comme la compétition entre la tension de ligne de la goutte et la force locale exercée sur la ligne par les défauts. Bien que les gouttes soient alimentées à débit constant, le mouvement de la ligne de contact est irrégulier, formé de sauts entre les différents sites d'accrochage. Sous certaines conditions, ces sauts sont corrélés en temps et en espace, conduisant à des phénomènes de type avalancheux et au déplacement à grande échelle du centre de masse de la goutte.
Mots-clés : mouillage, surfaces hétérogènes.

***Abstract* — *Spreading of Large Drops on Patterned Surfaces*** — *We report an experimental study of the shape of large liquid drops spreading on surfaces with patterns of wettability. The patterns are sets of disks of a material less wettable than the rest of the plane substrate. When few defects are present, or when the average distance between defects is large compared to the capillary length, the drop edge is a set of circular arcs connecting the pinning points. When the density of defects is smaller than the capillary length, the contact line shape is more complex and we analyze its morphology through a kind of box counting method. The roughness of the contact line is maximum when the average distance between defects is comparable to two times the defects size. Setting the non-wetting defects on a periodic or almost periodic array produces drops with faceted edges. The transition between circular and faceted drops can be understood as a competition between the tension of the drop edge and the local force exerted on the contact line by the defects. Although the drops are grown at a fixed flow rate, the motion of the contact line is irregular, with jumps between pinning sites. In some cases, the jumps of the contact line are correlated in space, leading to "avalanches" and large scale motions of the drop.*
*Keywords: wetting, heterogeneous surfaces.*

## INTRODUCTION

Spreading of liquid films on solid surfaces sometimes takes place on heterogeneous surfaces, with roughness and chemical heterogeneity. Coating processes are generally designed to leave a thin, uniform film on the solid surface. Formation of holes or unevenness of the coating may result in the failure of the function provided by the liquid film. It is thus important for these industrial processes to understand the influence of surface defects on the spreading of liquid films.

Recently, patterned surfaces with wettability contrast have been used to trap liquid droplets, in particular to create arrays of microreactors (Jackman *et al*., 1998; Gau *et al*., 1999). Numerous microfluidic devices have been developed recently, in particular for the analysis of biological molecules. Some of these devices rely on the existence of a wettability contrast on the substrate (Burns *et al*., 1998; Grunze, 1999) and their successful operation requires the understanding of the anchoring of the moving contact line motion on a wettability contrast line.

While the dynamics of wetting on a chemical homogeneous, smooth surface are well understood both at the macroscopic and microscopic levels (de Gennes, 1985; Leger and Joanny, 1992), wetting on heterogeneous surfaces still raises some questions. There are theoretical investigations of the distortion of a contact line due to wettability defect (Joanny and de Gennes, 1984; Pomeau and Vannimenus, 1985; Robbins and Joanny, 1987; di Meglio and Shanahan, 1993; Crassoux and Charlaix, 1994). In particular, Joanny and de Gennes showed early on (Joanny and de Gennes, 1984; de Gennes, 1985) that a contact line exhibits a peculiar elasticity that leads to a very large extension of the deformation due to a single defect. Another consequence of this peculiar elasticity is the long range interaction between defects on the substrate. The theoretical results are mostly limited to small deformations of the contact line, because the general problem is very difficult to solve analytically.

The deformation of the contact line due to a single defect was investigated in several experiments in a capillary rise situation (Cazabat and Heslot, 1990; Nadkarni and Garoff, 1992; Marsh and Cazabat, 1993) and in an "imperfect Hele-Shaw cell" geometry (Paterson *et al*., 1995). In these cases, the deformation is well described by existing analytical theories. The case of many defects was also investigated experimentally, again in a capillary rise situation (di Meglio, 1992; Decker and Garoff, 1997), in the imperfect Hele-Shaw cell (Paterson and Fermigier, 1997), for drops squeezed between solid surfaces (Chatain and de Jonghe, 1996) and more recently for wetting He films (Rolley *et al*., 1998).

In this paper, we report an experimental investigation of the spreading of large liquid drops on patterned surfaces with wettability defects. The typical diameter of the drops is larger than the capillary length so that most of the drop surface is flattened by gravity. The three-dimensional deformation induced by the surface defects is limited to the edge of the drop, but there are large scale deformations of the contact line. We study the morphology of the contact line as a function of the density, size and spatial distribution of non-wetting defects. We analyze first the influence of a very small number of defects acting as individual pinning points. Then we determine how many randomly distributed defects change the morphology of the contact line. We also analyze the dynamics of contact line jumps. Finally, we show that drops with faceted edges can be obtained when the defects are arranged in ordered (or nearly ordered) arrays.

## 1 EXPERIMENTAL SET-UP

The patterned surfaces are silicon wafers (diameter 10 cm) on which a thin layer (0.5 μm) of photosensitive resin (*Hoechst* AZ 4000) is spread by spin coating. This layer of resin is exposed to UV light through a mask made on a high-resolution (2400 dpi) laser printer. Parts of the resin layer that are exposed to UV are then removed from the silicon surface. The resulting surface is a set of circular dots of resin (with a low surface energy) on a silicon substrate (with a high surface energy). The contact angle of the liquid on the resin surface is $\theta_d = 78°$ and on the silicon surface $\theta_0 = 28°$. The difference in contact angles is clearly visible on the oblique view of the drop shown in Figure 1. The wettability contrast is defined as the difference of spreading coefficients between the defects and the silicon surface: $\Delta S = S_d - S_0 = \gamma(\cos\theta_d - \cos\theta_0)$. In the present experiments, this wettability contrast is: $\Delta S$ = 31.6 mN/m. A mixture of water and glycerin (composition: 60% glycerol, 40% water in volume, density $\rho$ = 1.153, surface tension $\gamma$ = 46.8 mN/m, viscosity: 0.011 Pa·s) is spread on the patterned surface. The liquid is driven at constant flow rate with a syringe pump. The average contact line velocity in the experiments is 10 μm/s, corresponding to a capillary number Ca ~ $10^{-5}$. The spreading process is monitored with either a conventional CCD video camera (512 x 512 pixels, with 256 gray levels) or a high-resolution digital camera (2032 x 2044 pixels, 1024 gray levels) located above the substrate. Images are digitized at equally spaced times during the experiment. One pixel in the image corresponds to 170 μm with the low-resolution camera and 17 μm with the high-resolution camera.

The digital pictures are processed to determine the location of the contact line as a function of time. The mask used to make the patterned surface is generated by a computer and the location of each defect is known. So, it is possible to superimpose the defect pattern on the images of the contact line *(see for example Fig. 2)*. The defect patterns are sets of identical circles located on a more or less disordered array. The location of the center of each defect has $x$ and $y$ coordinates such as: $x_i = n_i\, a + a\, no\, r_{xi}$ and: $y_i = m_i\, a + a\, no\, r_{yi}$, where $a$ is the mesh size of a square pattern, $no$ is a

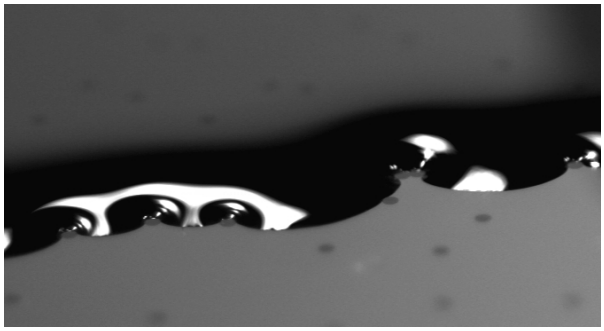

Figure 1

Oblique view of the edge of the drop. The darker circles on the substrate are the non-wetting defects. The change of contact angle on the defects is revealed by the change of light intensity reflected by the liquid-air interface.

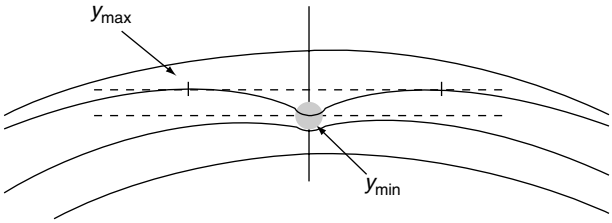


Figure 2

Pinning on a single defect.

randomness parameter (when $no = 0$, the pattern is perfectly ordered; when $no$ is much larger than 1, the pattern is a random set of circles), $n_i$ and $m_i$ are integer numbers, and $r_{xi}$ and $r_{yi}$ are random numbers evenly distributed between 0 and 1. The ratio between the mesh size $a$ and the defect diameter $d$ sets the surface fraction covered by the non-wetting resin $\sigma$. The randomness parameter changes the distribution of distances between nearest neighbor defects. It is possible to define an average distance between defects $d_{id}$ from the defect density $\sigma$. If we assume that there is no overlap between defects and that each defect of area $\pi d^2/4$ occupies the center of a square of size $a$, the surface fraction covered by the defect is: $\sigma = \pi d^2/4a^2$. In this case, the distance between nearest neighbor defects is $a$ and: $d_{id} = (d/2)\ (\pi/\sigma)^{1/2}$. This derivation assumes that there is no overlap between defects, which is only true at small values of $\sigma$. At larger values of $\sigma$, the actual fraction of the substrate covered by the less wetting material is smaller than $\pi d^2/4a^2$.

The statistics of arrays of disks randomly distributed on a plane were studied by Gawlinski and Stanley (1981). They showed in particular that the percolation threshold is: $\sigma = 0.72$. At this threshold, the size of the largest cluster (defined here as a set of overlapping disks) diverges.

## 2 ISOLATED DEFECTS

To understand the dynamics of the contact line and the shape of large drops spreading on rigid solid heterogeneous substrates, the knowledge of the dynamics of the contact depinning from a single defect is essential. The geometric feature of this process is a basic local phenomenon controlling the overall shape of the drop.

The dimensionless strength $f$ of the wettability defects is defined as: $f = d\ \Delta S/\gamma e$ where $d$ is the defect diameter, $e$ is the thickness of the drop, $\gamma$ is the surface tension of the liquid.

Experiments were performed varying the size of the defect from 0.1 to 1.8 mm, corresponding to a range of dimensionless force $f$ between 0.04 and 0.71. Figure 2 shows the deformation of the contact line on a single defect of diameter 0.6 mm. To quantify the deformation, we plot the positions $y_{min}$ and $y_{max}$ of the two horizontal tangents to the contact line. Figure 3 shows that the amplitude of line deformation is proportional to the defect size $d$ when $f < 0.5$. When $f > 0.5$, the deformation of the contact line increases with the defect force until $f \sim 1$, then the defect traps the contact line and remains non wetted by the liquid. For small defect forces, the shape of the contact line is homothetic to the center of the defect and the magnification factor is proportional to the defect force. Therefore, it is possible to characterize this shape by a geometric parameter: the depinning angle $\delta_0$. This angle is defined as the angle between the two tangents to the contact line on each part of the defect, whose intersection is the center of the contact line anchored to the defect. This angle is measured just before the triple line begins to advance on the defect. This depinning angle remains constant for small defect forces.

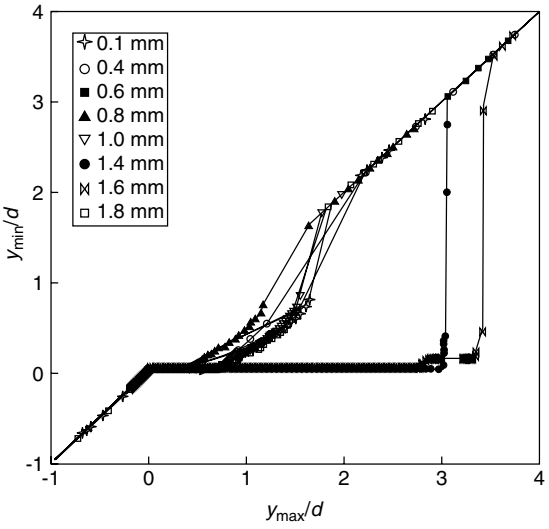


Figure 3

Position of the bottom tangent to the contact line *vs*. position of the top tangent. Both positions normalized by defect diameters.

## 3 MANY DEFECTS: INFLUENCE OF DEFECT DENSITY ON DROP MORPHOLOGY

We investigated the change in drop shape as we change the density of defects on the substrate while keeping the randomness of the distribution constant. We start with a density of defects $\sigma_{min} = 0.016$ and increase it up to $\sigma_{max} = 0.785$. At the lowest density, the mean distance between nearest neighbor defects is larger than the capillary length and the probability of forming clusters of defects is very small. The defects act as pinning points for the contact line, which is still a set of circular arcs but with randomly distributed lengths *(Fig. 4)*. When the defect density is increased beyond $\sigma = 0.031$, the mean distance between defects becomes smaller than the capillary length and defects begin to act collectively on the contact line *(Fig. 5)*. On the other hand, the probability of formation of defect clusters increases. At very low defect concentration, there is only a fluctuation in the position of the pinning points, but all defects have the same strength. As the defect density is increased, the contact line fluctuations occur at smaller and smaller length scales *(Figs. 6-9)*.

### 3.1 Analysis of Contact Line Morphology

As can be seen in Figures 4-9, the overall shape of the drop can be quite different from a circle. It is then impossible to analyze the fluctuations of the contact line by simply comparing the actual position of the line to a disk of equivalent area. To give a quantitative description of the changes in contact line shape when the defect density is changed, we measure the contact line length with a ruler of varying size $L$.

For each record in time, the contact line is approximated by a polygon whose sides have a length $L$. This construction is illustrated in Figure 10. The values of $L$ range from the pixel size to several times the capillary length $\lambda_c$. As expected, the measured perimeter decreases when $L$ is increased for every value of the defect density $\sigma$ *(Fig. 11)*. The decay of the perimeter as a function of $L$ is slowest for the uniform substrates ($\sigma = 0$ and $\sigma = 1$) when the drop edges are circular. In these two cases, the decay corresponds to the change in perimeter of regular polygons included within a circle of radius $R$: the relative perimeter $p_r$ (ratio of the polygon perimeter to the circle perimeter) is:

$$p_r = \left(\frac{L}{2R}\right)\arcsin\left(\frac{L}{2R}\right)$$

The decay of the perimeter is fastest for intermediate values of the defect density. This can be seen in Figure 11 by plotting on a log-log graph the perimeter dependence on the length measurement. The slope $p$ of each curve corresponds to $p = 1 - d_f$, where $d_f$ is the fractal dimension. In Figure 12 is plotted the fractal dimension *versus* the defect density. The values of the fractal dimension are very close to the unity so the shape of the contact line is not strictly speaking a fractal, on the other hand the fractal dimension is a way to characterize the roughness of the line.

There are two different systems.

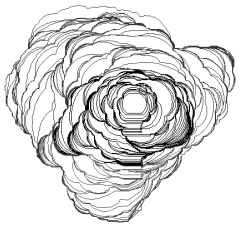

Figure 4

$\sigma = 0.016$.

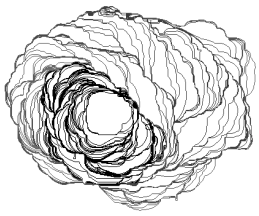

Figure 5

$\sigma = 0.031$.

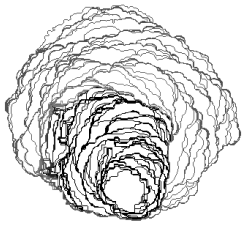

Figure 6

$\sigma = 0.130$.

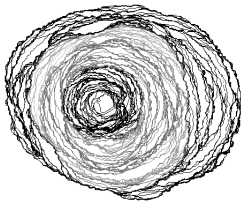

Figure 7

$\sigma = 0.250$.

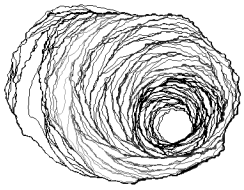

Figure 8

$\sigma = 0.500$.

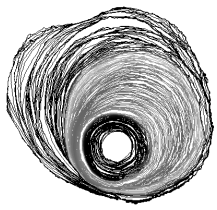

Figure 9

$\sigma = 0.785$.

Figures 4-9

Influence of the defect density $\sigma$ on the shape of drops (defect size $d = 0.4$ mm; randomness parameter $no = 4$).

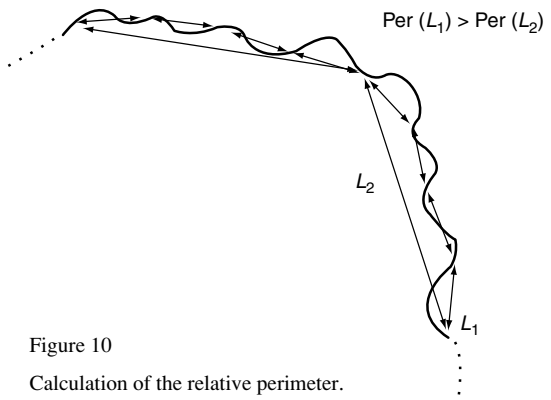


Figure 10

Calculation of the relative perimeter.

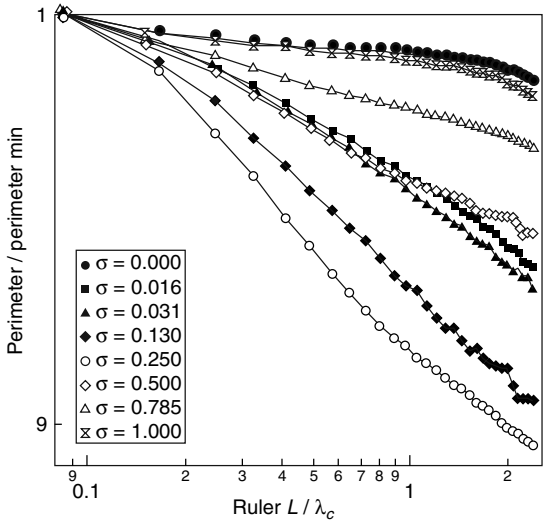


Figure 11

Relative perimeter for different defect densities.

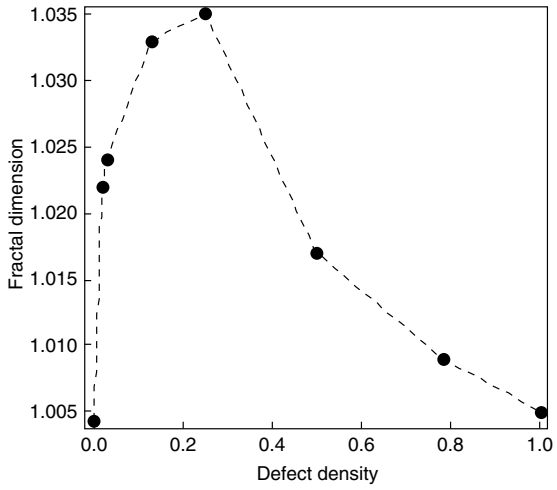


Figure 12

Fractal dimension (roughness) *vs.* defect density.

For small defect density (from $\sigma = 0$ to 0.25) defects are diluted on the substrate, they act individually on the shape of the contact line. So increasing defect density increases the roughness of the contact line.

For high defect density (from $\sigma = 0.25$ to 1) collective effects play an important part on the shape of the line. As can be seen in Figure 1, each defect deforms the liquid-air interface over a distance depending on the defect force. Experiments were performed to study the coupling between two defects on the shape of the contact line varying the distance between defects from $10d$ to $1.5d$ ($d = 0.4$ mm). These experiments showed that when the distance between the defects is about $2d$, the contact line averages its deformation on the two defects as one large defect. So, below a distance of $2d$ between two defects of size $d$, the defects are forming a cluster for the contact line. For the experiments varying the defect density, the fact that the roughness has a maximum for $\sigma = 0.25$ corresponding to a mean distance between defects of about $2d$ indicates that defects are forming clusters for the contact line. Increasing defect density means decreasing the mean distance between defects, therefore the contact line roughness decreases as more and more defects are forming clusters.

It can be seen from Figure 11 that the relative perimeter is lowest for the defect densities $\sigma = 0.063$, 0.13 and 0.25, corresponding to average distances between defects $0.7\lambda_c$, $0.5\lambda_c$ and $0.35\lambda_c$. This shows that the fluctuations of wettability are most effective to create fluctuations of the contact line when the mean distance between defects is slightly lower than the capillary length. We think that this is consistent with the analysis of Pomeau and Vannimenus (1985) for a single defect on a vertical substrate. In our case, at defect densities larger than 0.25, the contact line "sees" an averaged fluctuation of the spreading coefficient, with a smaller amplitude. As a result, the contact line fluctuations are lower.

## 3.2 Global Motion of the Drop

In most of the experiments, a global motion of the drop can be observed. More precisely, if we determine the location of the center of gravity of the drop, defined as the average $x$ and $y$ positions of all pixels contained within the contact line, we can follow the motion of this center of gravity during the spreading experiment. Such a global motion is shown in Figure 13 with the corresponding evolution of contact lines in Figure 14, for a disordered distribution of defects ($no = 4$) and a small surface fraction of defects $\sigma = 0.016$ corresponding to a mean distance between defects $d_{id} = 1.4\lambda_c$. A global drop motion implies that the resulting force on the drop edge is non zero. The defects are evenly distributed on the substrate if one looks at this distribution at a length scale larger than the mean distance between defects. An analysis of the active sites on the contact line reveals that a coherent

motion of the drop is related to the correlation of active sites. To show this correlation, we make activity diagrams for the moving contact line. An active site is defined as a point on the contact line moving in a given time $\Delta t$ over a distance larger than a given threshold. Here the minimum time interval is determined by the digitizing interval during the experiment (30 s). The minimum distance to test the contact line motion is determined by the pixel size. To make the activity diagram shown in Figure 15, we use polar coordinates as defined in Figure 14, taking the origin of radial coordinate at the point where the liquid is injected. For each point on the contact line, at a given time $t_n$, we determine the distance traveled, in a direction perpendicular to the contact line at that point, between time $t_n$ and time $t_{n+1} = t_n + \Delta t$. The activity diagram is a false color image where the $x$ and $y$ coordinates are proportional to the angular and radial coordinates and the color (from black to white) codes the amplitude of motion.

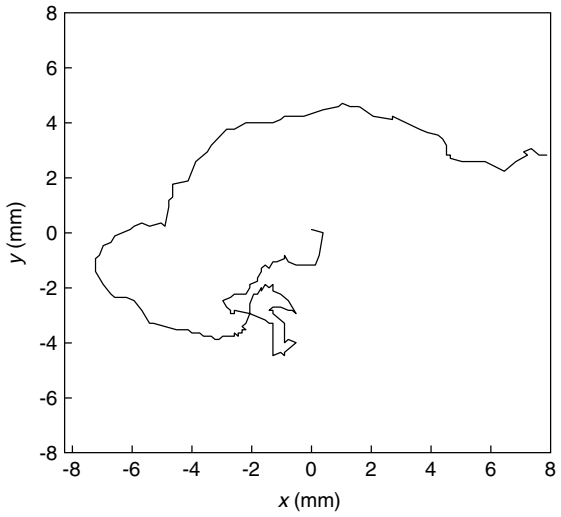


Figure 13

Motion of the center of gravity.

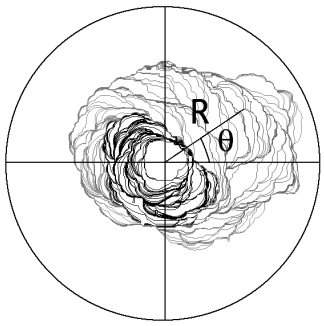


Figure 14

Evolution of the contact line.

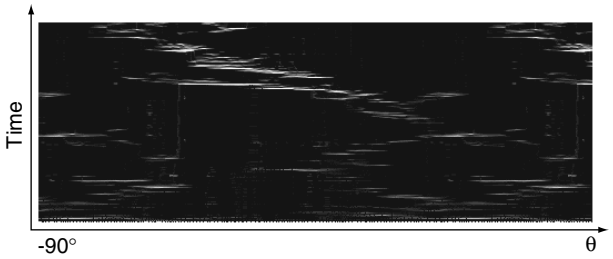


Figure 15

Activity diagram.

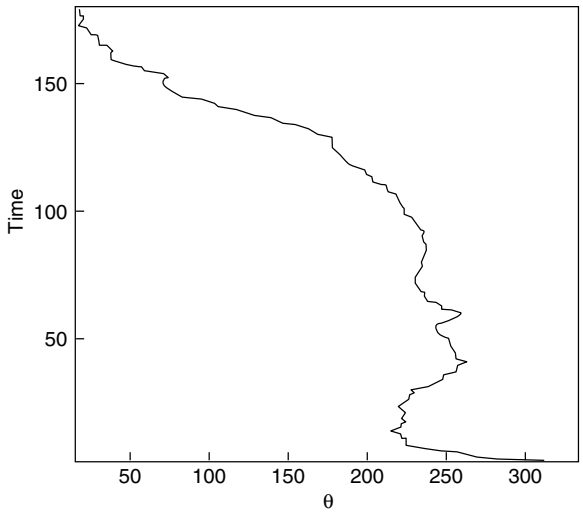


Figure 16

Motion of the center of mass in polar coordinates.

The motion of the contact line is localized in space although the liquid is injected at constant flow rate. Very often, a motion of large amplitude at a given time triggers the motion in the vicinity at later times. This localized, correlated motion results in a displacement of the center of mass of the drop. The relation between the active sites and the motion of the center of mass is clearly seen when we plot the latter in the same radial coordinates *(Fig. 16)*. In particular, in the upper part of the activity diagram, there is a band of strong motion going from right to left. At the same time, the center of mass follows the direction of this activity band.

The motion occurs where the contact line feels the smallest resistance and, since the defects are randomly distributed on the substrate, active sites should *a priori* not be correlated. It is not yet clear why the motion of the contact line at a given point triggers motion preferentially in the immediate vicinity. There are two possible explanations for these correlations: dynamic transient effects due to the sudden depinning of the line, or a biased sampling of the substrate due to the mechanism of the drop motion itself. In

other words, it could be either a change in the line trapping condition due to the high transient velocities achieved just after depinning or a redistribution of local stresses on the contact line.

The flow rate is very small and the Reynolds number based on the mean velocity of the contact line and the drop height is in the order of $10^{-4}$. But, when the contact line is released from a defect, the local velocity is much larger than the average velocity. The dynamics of contact line depinning from a single defect has already been studied theoretically (De Gennes, 1985) and experimentally (Marsh and Cazabat, 1993) in the case of small contact angles. The transient depinning velocity is determined by the characteristic velocity $U^* = \gamma/\eta$ and geometrical factors, mainly the contact angle. In our case the velocity $U^*$ is around 4.2 m/s and it corresponds to a Reynolds number in the order of 40. However, in the experiments, the contact line velocity immediately after depinning remains far below the characteristic velocity $U^*$, since it is typically a few mm/s, and the corresponding Reynolds number is still much less than one.

The other possible cause of a coherent motion of the contact line is a "memory effect", as described by Caldarelli *et al*. (1998) in the context of fracture propagation in disordered media. Given two defects with different force thresholds for depinning, if the contact line depins from the weaker defect, the probability of depinning from the stronger one, conditioned by that first event, is decreased. In other words, if the contact line is, at a given time, pinned at some location *A* and moves to other locations *B*, the contact line has a larger probability of continuing to move at *B* than starting to move at *A*.

### 3.3 Average Contact Angle

As the surface fraction of non-wetting material is increased, we expect the average contact angle to increase too. There are several ways to define this average angle. One could follow exactly the contact line on the heterogeneous substrate and measure the contact angle at each location: equal to $\theta_0$ when the line is on the clean substrate, equal to $\theta_d$ when the line is on a defect and intermediate between $\theta_0$ and $\theta_d$ when the contact line is pinned on a defect edge. This method is difficult to implement and we choose another definition, which is not strictly equivalent. Since the drops are much wider than $\lambda_c$, they are flat except near the edges. We can use the relation between equilibrium thickness and contact angle, derived for a homogeneous substrate, to define the average contact angle $\theta_m$ as:

$$\theta_m = 2\arcsin\left(\frac{e}{2\lambda_c}\right)$$

At the end of each experiment, when the drop is largest, we measure the drop thickness, at several points near the center of the drop, mechanically with an accuracy of 0.01 mm. This drop thickness is plotted as a function of defect density for the different defect sizes that we used *(Fig. 17)*. If we assume that the contact line does a random sampling of the heterogeneous surface, we expect that the spreading coefficient seen by the line will be an average of the spreading coefficients on the clean substrate and on the defects, weighted by their respective surface fraction. This is Cassie's law, which can be expressed as:

$$\cos\theta_c = \sigma\cos\theta_d + (1-\sigma)\cos\theta_0$$

Cassie's law has been recently observed on substrates with microscopic heterogeneities (Langmuir-Blodgett films deposited on silicon, self-assembled monolayers of mixed thiolates on gold) (Semal *et al*., 1999). It can be seen from our data than in the case of macroscopic heterogeneities, the average contact angle deduced from the drop thickness does not follow Cassie's law. Other experiments, done by dipping a heterogeneous surface into a bath of liquid, reveal a similar behavior (Paterson *et al*., 1998). These experiments in the Wilhelmy plate geometry showed also that both receding and advancing contact angles depend on the disorder of the defect distribution. In our experiments with large sessile drops, the contact angle is larger than predicted by Cassie's law, particularly at small defect density. It can be seen that there is a large fluctuation of the drop thickness at a given defect density when we change the defect size or the defect spatial distribution (see data at $\sigma = 0.5$ in Figure 17).

We can interpret this departure from Cassie's law as the result of the inability for the contact line to reach an equilibrium position (*i.e*. a position corresponding to an energy minimum with the constraint of fixed liquid volume).

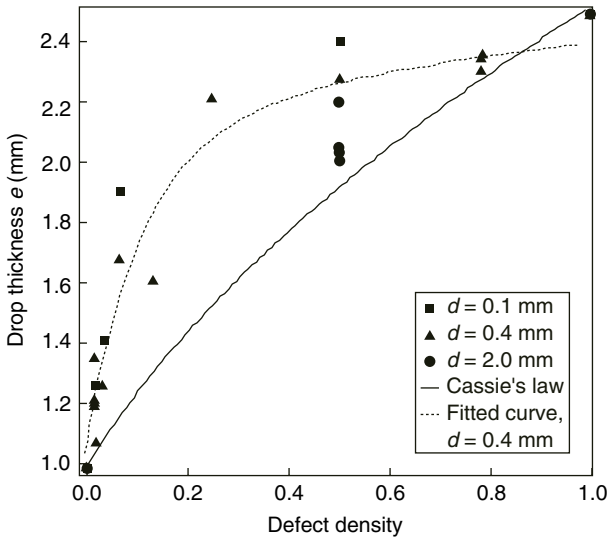


Figure 17

Drop thickness *vs*. defect density.

By superimposing the location of the contact line and the edges of the defects (image recorded prior to the spreading of the liquid), we can see that the contact line is preferentially anchored on the defect edges. Thus the contact line "oversamples" the regions of the substrate where the contact angle is high, compared to a straight line that would measure the true average contact angle.

## 4 FACETED DROPS

When defects are set on a periodic or almost periodic array the shape of the drop keeps the symmetry of the substrate if the defect forces are large enough. This phenomenon results from the competition between line tension (minimizing the free surface, the 2D shape of the drop is as compact as possible) and surface energy barriers on the substrate (defects are located on rows, the rows with the maximum density of defect have the highest surface energy barriers) (Cubaud and Fermigier, 2000). An example of a drop sitting on a hexagonal array of small defect is shown in Figure 18. As can be seen from this oblique view, the edges of the drop are straight and they form an almost perfect hexagon.

It is possible to initiate a transition between circular and faceted drops varying defect force. Experiments were performed on a square array varying defects size from 0.5 to 2 mm, corresponding to a range of dimensionless force $f$ between 0.14 and 0.58. The shape of defect is a square and the wettability contrast is inverse compared to the experiments described above (defects are wetting). As can be seen in Figures 19a to 19d the shape of the drop is modified as a function of defect force. For small defect force, the shape of the drop seen at a length scale larger than the capillary length is not affected by the surface topography. Increasing defect force, the macroscopic shape changes from a circle to a square according to each square pattern.

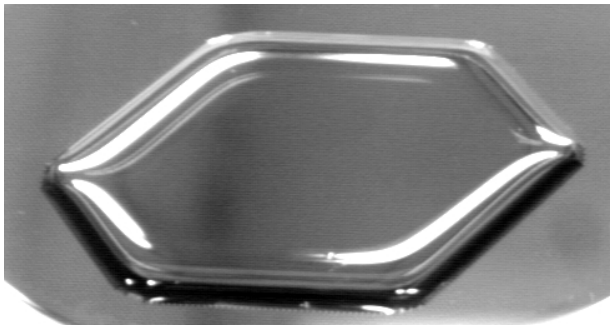

Figure 18

Large sessile drop setting on a hexagonal array of small non-wetting defects ($d$ = 0.4 mm). The size of the drop is 3 cm.

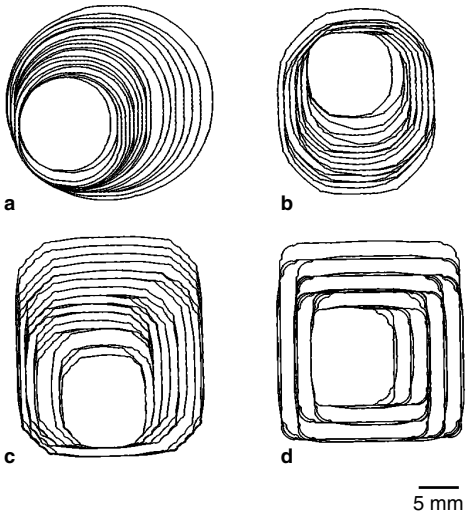


Figure 19

Morphologic evolution of a drop setting on different square patterns with different defect sizes.
(a) $d$ = 0.5 mm, $f$ = 0.14. (b) $d$ = 0.707 mm, $f$ = 0.20. (c) $d$ = 1 mm, $f$ = 0.29. (d) $d$ = 2 mm, $f$ = 0.58.

## CONCLUSION

The data obtained on the shape of the contact line anchored to a single defect suggests that, for small defects (dimensionless force less than 0.5), the maximum amplitude of deformation and the lateral extent are proportional to the defect size.

We have shown experimentally the existence of faceted liquid drops when macroscopic wettability defects are ordered on plane substrate and the transition between circular and faceted drops when the defect force is varied.

The collective motion of the contact line results from the kind of pinning of defects on the contact line. When the defect density is low, the thickness of the drop is low *(Fig. 17)* then the defect force is higher than for a high density of defect. The defects have a strong pinning on the contact line. Therefore, the depinning sites are essentially individual. When a depinning occurs, it is able to disturb the local configuration of the line and to spread as a "waterfall" to the rest of the line. This way the center of mass of the drop follows the direction of the strongest activity. For a high density of defects, the weak pinning of defect controls the motion of the contact line. The coupling between defects is strong and there is some collective depinning.

There is a maximum of roughness for the contact line varying the defect density for a fixed size of defects. This maximum results from the coupling between defects *via* the contact line and could be considered as a frontier between individual and collective pinning.

## ACKNOWLEDGEMENTS

We acknowledge financial support from *Institut français du pétrole*. The patterned substrates were prepared in *CNRS,* Laboratoire de microélectronique et microstructure with the help of D. Mailly.

## REFERENCES

Burns, M.A., Johnson, B.N., Brahmasandra, S.N. and Handique, K. (1998) An Integrated Nanoliter DNA Analysis Device. *Science*, **282**, 484-487.

Caldarelli, G., Cafiero, R. and Gabrielli, A. (1998) Dynamics of Fractures in Quenched Disordered Media. *Phys. Rev. E*, **57**, 4, 3878-3885.

Cazabat, A.M. and Heslot, F. (1990) Wetting in Non-homogeneous Situations. *Colloids and Surfaces*, **51**, 309-322.

Chatain, D. and de Jonghe, V. (1996) Chemical Wetting Hysteresis. *J. Adhesion*, **58**, 163-171.

Crassoux, J. and Charlaix, E. (1994) Contact Angle Hysteresis on a Heterogeneous Surface: Solution in the Limit of a Weakly Distorted Contact Line. *Europhys. Lett*., **28**, 6, 415-420.

Cubaud, T. and Fermigier, M. (2000) Faceted Drops on Heterogeneous Surfaces. *Europhys. Lett*. (submitted).

Decker, E.L. and Garoff, S. (1997) Contact Line Structure and Dynamics on Surface with Contact Angle Hysteresis. *Langmuir*, **13**, 6321-6332.

De Gennes, P.G. (1985) Wetting: Statics and Dynamics. *Rev. Mod. Phys*., **57**, 3, 827-863.

Di Meglio, J.M. (1992) Contact Angle Hysteresis and Interacting Surface Defects. *Europhys. Lett.,* **17**, 607-612.

Di Meglio, J.M. and Shanahan, M.E.R. (1993) Effets coopératifs de défauts sur l'angle de contact : le phénomène d'ombrage. *C.R. Acad. Sci. Paris*, **316**, Série II, 1543-1548.

Gau, H., Herminghaus, S., Lenz, P. and Lipowsky, R. (1999) Liquid Morphologies on Structured Surfaces: From Microchannels to Microships. *Science*, **283**, 46-49.

Gawlinski, E.T. and Stanley, H.E. (1981) Continuum Percolation in Two Dimensions: Monte Carlo Tests of Scaling and Universality for Non-Interacting Disks. *J. Phys. A*, **14**, L291-L299.

Grunze, M. (1999) Driven Liquids. *Science*, **28**, 41-42.

Jackman, R.J., Duffy, D.C., Ostuni, E., Willmore, N.D. and Whitesides, G.M. (1998) Fabricating Large Arrays of Microwells with Arbitrary Dimensions and Filling Them Using Discontinuous Dewetting. *Anal. Chem*., **70**, 2280-2287.

Joanny, J.F. and de Gennes, P.G. (1984) Model for Contact Angle Hysteresis. *J. Chem. Phys*., **11**, 552-562.

Leger, L. and Joanny, J.F. (1992) Liquid Spreading. *Rep. Prog. Phys*., **55**, 431-486.

Marsh, J.A. and Cazabat, A.M. (1993) Dynamics of Contact Line Depinning from a Single Defect. *Phys. Rev. Lett*., **71**, 15, 2433-2436.

Nadkarni, G.D. and Garoff, S. (1992) An Investigation of Microscopic Aspects of Contact Angle Hysteresis: Pinning of the Contact Line on a Single Defect. *Europhys. Lett*., **20**, 6, 523-528.

Paterson, A. and Fermigier, M. (1997) Wetting of Heterogeneous Surfaces: Influence of Defect Interaction. *Phys. Fluids*, **9**, 8, 2210-2216.

Paterson, A., Fermigier, M., Jenffer, P. and Limat, L. (1995) Wetting of Heterogeneous Surfaces: Experiments in an Imperfect Hele-Shaw Cell. *Phys. Rev. E*, **51**, 1291-1298.

Paterson, A., Robin, M., Fermigier, M., Jenffer, P. and Hulin, J.P. (1998) Effects of Density and Spatial Distribution of Wettability Heterogeneities on Contact Angle. *J. Petroleum Sci. Eng*., **20**, 127.

Pomeau, Y. and Vannimenus, J. (1985) Contact Angle on Heterogeneous Surface: Weak Heterogeneities. *J. Colloid Interface Sci*., **104**, 477-488.

Robbins, M.O. and Joanny, J.F. (1987) Contact Angle Hysteresis on Random Surfaces. *Europhysics Lett*., **3**, 729-735.

Rolley, E., Guthmann, C., Gombrowicz, R. and Repain, V. (1998) The Roughness of the Contact Line on a Disordered Substrate. *Phys. Rev. Lett*., **80**, 13, 2865-2868.

Semal, S., Voué, M. and De Coninck, J. (1999) Dynamics of Spontaneous Spreading on Energetically Adjustable Surfaces in a Partial Wetting Regime. *Langmuir*, **15**, 7848-7854.

*Final manuscript received in September 2000*